To the Graduate Council:

I am submitting herewith a thesis written by Caitlin Bunce entitled "Lower Limits of Performance of an Electrospray Thruster using a Direct Measurement Method." I have examined the final paper copy of this thesis for form and content and recommend that it be accepted in partial fulfillment of the requirements for the degree of Master of Science, with a major in Aerospace Engineering.

Dr. Trevor Moeller, Major Professor

We have read this thesis
and recommend its acceptance:

Dr. Trevor Moeller

Dr. Brian Canfield

Dr. Lino Costa

Accepted for the Council:

Dixie L. Thompson

Vice Provost and Dean of the Graduate School

To the Graduate Council:

I am submitting herewith a thesis written by Caitlin Bunce entitled "Lower Limits of Performance of an Electrospray Thruster using a Direct Measurement Method." I have examined the final electronic copy of this thesis for form and content and recommend that it be accepted in partial fulfillment of the requirements for the degree of Master of Science, with a major in Aerospace Engineering.

Dr. Trevor Moeller, Major Professor

We have read this thesis
and recommend its acceptance:

Dr. Trevor Moeller

Dr. Brian Canfield

Dr. Lino Costa

Accepted for the Council:

Dixie L. Thompson

Vice Provost and Dean of the Graduate School

(Original signatures are on file with official student records.)

Lower Limits of Performance of an Electrospray Thruster using a Direct Measurement Method

A Thesis Presented for the

Master of Science

Degree

The University of Tennessee, Knoxville

Caitlin Bunce

May 2024

I dedicated this thesis to my father, Scott Bunce. Your confidence in me has pushed me to become the woman I am today.

Acknowledgements

I would like to express my gratitude to my advisor and committee member, Dr. Trevor Moeller. His passion for the work inspired me to pursue my education at the University of Tennessee Space Institute. His guidance during my application process and his work to ensure there was a place for me in the CEAR group was crucial to my success. From the classroom to graduate research work and beyond, his advice and expertise has been endlessly helpful, and I am grateful to have such an advisor during my time here.

I would also like to thank my other committee members, Dr. Brian Canfield and Dr. Lino Costa. Dr. Canfield has always been available to answer my endless questions and help me understand a given topic on a deeper level and see why it is important. Dr. Costa has always pushed me to look at engineering problems in creative ways that haven't been considered before. Both their time and guidance are greatly appreciated. I would also like to thank Alex Terekhov for his continuous help in setting up experiments and providing ideas to remedy issues I faced.

Additionally, I would like to thank the administration at UTSI for creating a positive environment for me and the other students throughout our time here. I would also like to thank my fellow graduate research assistants in the CEAR group for the brainstorming, ideas, and insights, as well as the GRA's from other groups for creating a fun and positive environment. It has been a privilege to work alongside such talented people.

I would also like to thank the Tennessee NASA Space Grant, award number 80NSSC20M0126, for the funding that allowed me to be involved in the μSTAMPS work at UTSI and pursue a topic in propulsion, which was everything I hoped for.

And last but not least, I would like to thank my friends and family for their endless love and support. My parents and three brothers have supported every dream I wanted to pursue, and it is because of their support that I am the engineer I am today. Their support also allowed me to push the boundaries of what I believed I was capable of and to tackle my dream of flight training while working on this thesis. My friends have also helped me tremendously by picking me up during the hard times and celebrating with me in the good times. Without them, none of this would be possible.

Abstract

Nanosatellites are a growing technology that offer a more accessible way for scientific missions to be conducted in space. The number of nanosatellites launched annually continues to grow, increasing the need for a propulsion system onboard to assist in collision avoidance, station keeping, rendezvous, and other attitude adjustments. More importantly though, new rulings have dictated that all orbiting spacecraft must deorbit within five years of mission completion to help mitigate the ever-growing problem of space debris. Electrospray thrusters, a subset of electric propulsion, is a well-researched method of propulsion for nanosatellites, including the novel μSTAMPS thruster currently in development at the University of Tennessee Space Institute (UTSI). Among the characteristics of these types of thrusters are high specific impulse with low thrust, and therefore, low thrust to weight ratios. Performance characterization is imperative to ensure a given mission can be completed without adding any more mass from propellant than is required. Traditionally, thrust stands are based on a torsional balance, hanging pendulum, or inverted pendulum approach, all of which required extensive and complex calibration and damping systems to resolve the forces expected from electrospray thrusters. The objective of this work is to determine the lowest level of thrust that can be measured by a simpler direct measurement technique involving the use of a weigh cell. This work focuses on the experimental set-up to baseline the selected weigh cell and determine the lowest level of thrust that is accurately measurable. The lowest thrust level measured was an impressive 1 μN. The μSTAMPS is anticipated to produce measurable force under

its current design. This work will then go on to make recommendations for future improvements.

Table of Contents

List of Tables

List of Figures

Chapter 1

Introduction

1.1 Background and Motivation

Nanosatellites, or nanosats, are an evolving category of small satellites with low mass, weighing between one and ten kilograms including propellant (wet). The low mass associated with nanosatellites widens the accessibility of scientific missions for research, exploration, defense, and many other applications.

Small satellites are used for a wide variety of applications, primarily in Low Earth Orbit (LEO). Among the most common applications are earth observation and monitoring, communications, and surveillance. Though LEO operations are the most prevalent, small satellites are also finding a place in deep-space missions as emerging technologies advance. One example of such a mission is the inclusion of the Light Italian Cubesat for Imaging of Asteroids (LICIA Cube) during NASA's Double Asteroid Redirection Test (DART) that was launched in November 2021 and concluded in September 2022. The LICIA Cube was separated from the redirecting space craft, using its own propulsion system, and the payload aboard imaged the collision and confirmed impact [3]. The LICIA Cube utilizes a 6U Cubesat and weighs in at just under 13 kg, so it is not technically in the nanosat category, but it is easy to see how important propulsion systems will be for deep-space missions as technology continues to get smaller, lighter, and more powerful.

The inclusion of an onboard propulsion system clearly widens the range of possibilities for this category of satellite. A propulsion system allows for maneuverability of the spacecraft for collision avoidance, station keeping, deorbit, and rendezvous. However, as of January 2024, only approximately 8% of nanosatellites launched include an onboard propulsion system [14]. A propulsion system also allows for the successful deorbit of the spacecraft after mission completion to help mitigate the growing issue of space debris. As of September 2022, the Federal Communications Commission (FCC) adopted a new rule that all spacecraft have a maximum post-mission lifetime of five years, down from the previous 25 years [5]. This time frame is incredibly difficult to achieve from most altitudes without a system on board to facilitate deorbit, whether that is via aerodynamic drag or propulsion.

As more and more nanosatellites are launched with propulsion systems on board to meet new regulations, have a more sophisticated and technically capable spacecraft, or push the boundaries of scientific missions in space, the need for accurate propulsion testing increases drastically. The goal of this work is to lay the foundation for a simple, effective, and accurate thrust-level testing method, and then determine the lowest thrust measurable with such a method.

1.2 μSTAMPS Overview

A thruster concept currently under development at UTSI is known as Micro Scalable Thrusters for Mission Profiles in Space, or μSTAMPS [7]. μSTAMPS is a novel design that operates on electrospray principles, which will be discussed further in Section 1.2.1, and is characterized by low thrust and high specific impulse, which is a measurement in seconds that indicates how long one kilogram of propellant can produce one newton of force. With the high cost typically associated with a launch, size and mass of propellant and hardware is critical to ensure as much of the available mass as possible is devoted to the payload or scientific mission. To ensure adequate propellant is onboard for the desired maneuvers, measurement of certain parameters relating to thruster performance are crucial, namely thrust and specific impulse.

1.2.1 Electrospray and Ionic Liquid Overview

The μSTAMPS thruster in development operate as an electrospray thruster. Electrospray thrusters are a subset of electric propulsion that are characterized by low thrust, high specific impulse, and small size, which makes them ideal for use on micro- and nanosatellites. Figure 1.1 shows thrust and specific impulse ranges for electrospray compared to other in-space propulsion modes. The principle of electrospray is well-established and becoming more relevant as MEMS (Micro-Electro-Mechanical Systems) technology advances, allowing satellites to become smaller and lighter.

Electrospray thrusters operate on electrodynamic principles. A conductive liquid, typically an ionic liquid, which is a salt with a low melting point (below 100 °C), is stored in a reservoir within the device or is delivered to the device from a propellant management system, which may include an external propellant tank, valves, regulators, plumbing to the device, and occasionally heaters to (re)liquify the propellant, if needed. A high electric field is applied via a voltage differential between the fluid and an extraction grid [23]. The balance between the applied electric force and surface tension induces a Taylor cone that creates charged particles that are accelerated in the electric field before ejection from the device, propelling the spacecraft forward [23]. A schematic of the general operation of an electrospray thruster can be seen in Figure 1.2.

Ionic liquids are typically used as propellants in electrospray propulsion, which contain exclusively, or almost exclusively, cations and anions, and are therefore ambipolar and conductive.

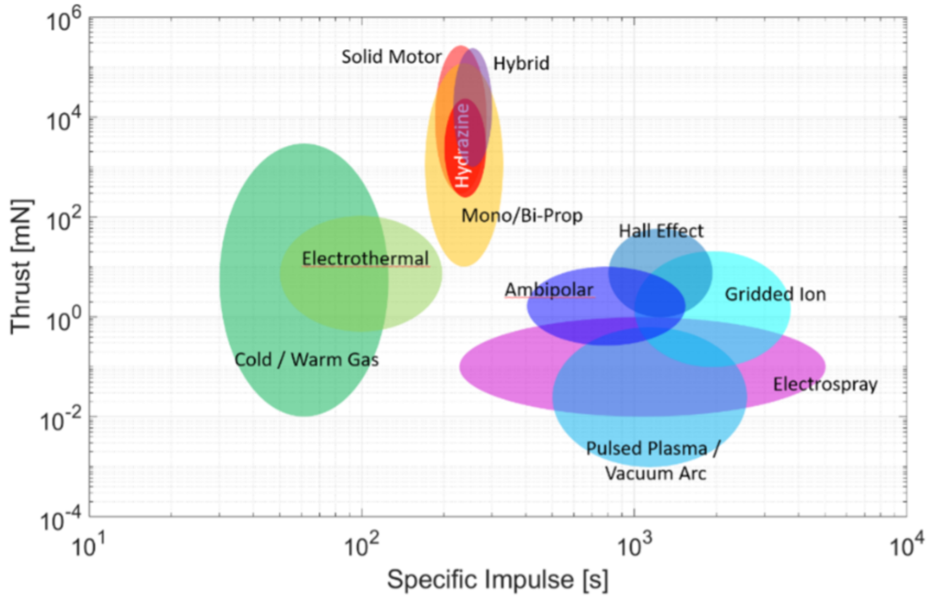

Figure 1.1: Thrust vs. specific impulse data for various in-space propulsion modes. [4]

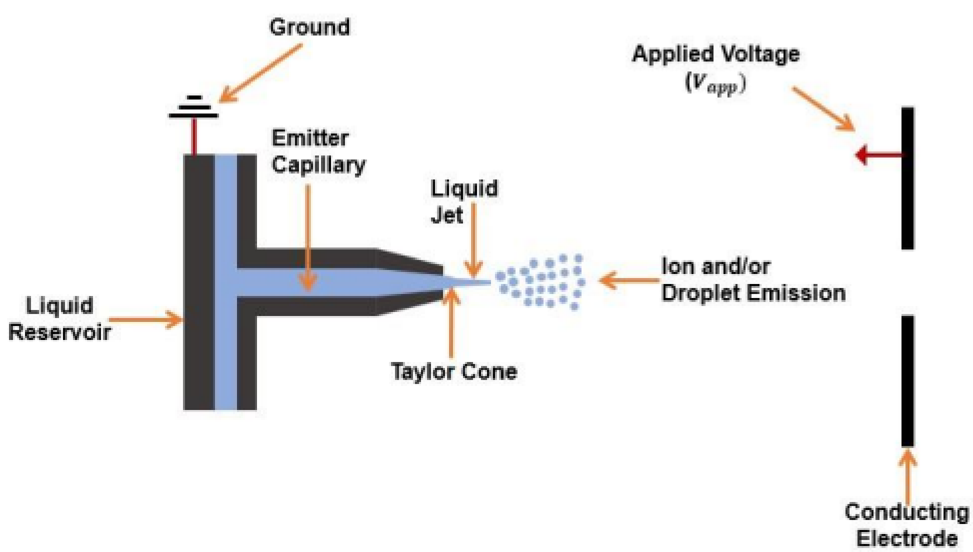

Figure 1.2: General electrospray schematic. [12]

This property allows electrospray thrusters to be operated in a pulsed mode by switching between positive and negative polarities, which sequentially extracts both species of ion, preventing both electric potential imbalance in the remaining propellant and electric charging of the spacecraft itself, and eliminating the need for a charge neutralizer [13]. One of the reasons most noted for the use of ionic liquids as a propellant is vapor pressure. The vapor pressure of ionic liquids is negligible at ambient pressures and temperatures due to the Coulomb force present between the cations and anions in the liquid, so they generally will not evaporate, making them ideal for vacuum environments. [10]. They are also thermally stable, remaining in liquid form across a wide range of temperatures [17].

1.2.2 μSTAMPS Design

The μSTAMPS thruster is an electric micro-propulsion device for small satellites being developed at UTSI based on the concept of electrospray propulsion [13]. The design consists of microchannels, or capillaries, that have an ultra-high aspect ratio and are embedded in a dielectric material, rather than protruding capillaries. This design eliminates the risk of breakage or surface erosion damage to a protruding capillary, which is a common failure pathway associated with typical micro-propulsion devices [21].

It was determined through electrostatic computational modelling work that an operating voltage as low as 200 volts is possible for this system, whereas many electrospray propulsion devices operate at a minimum of 1,000 volts [13]. This is an important advancement because the power and mass budgets can be lowered and allow for more of the volume within the satellite to be dedicated to the payload. The computational modeling established an ideal pitch distance between emitters for the lowest onset voltage of least 1.5 times the height of the capillaries [13]. The capillaries in the current design are 170 μm in height, and just 1 μm in diameter, with a pitch between capillaries of 255 μm. The capillaries are formed by Bessel-beam laser micro-machining in a class 1000 clean room using an ultra-fast 20 W Amplitude TANGERINE laser [13]. A schematic depicting the capillary geometry for a single capillary is shown in Figure 1.3 and the target dimensions are shown in Figure 1.4. The electrospray cavity is implemented to mitigate the risk of in the case of the ionic liquid propellant spilling. Howell conducted work to determine the dimensions of 'd' and 'm' of the electrospray cavity that minimize operating voltage [12].

The capillary is in hydraulic contact with the ionic liquid that is stored within a quartz fritted porous disc [13]. Dozens of standard height and diameter options exist for this quartz disc, which will allow for the thruster to be scalable to best fit the requirements of a given satellite and mission. The propellant flows from a porous disc into the capillaries via capillary action. As with traditional electrospray propulsion devices, the voltage differential applied between the propellant and the extraction grid forms a Taylor cone and produces thrust through the emission and acceleration of ions.

The extraction grid has an electrically conductive oxide coating, indium tin oxide (ITO) deposited directly on the dielectric material [13]. Borosilicate glass was chosen as the dielectric material due to the number of well-known micro-processing techniques, and it is suitable for space environments that may even eliminate effects of spacecraft charging [13]. The number of capillaries can be scaled up or down to produce a desired thrust level, and up to several thousand capillaries on a single emitter chip are feasible. The basis of this work is determining the smallest number of capillaries that can produce a measurable thrust level using direct measurement with the force balance.

Figure 1.5 shows an exploded CAD model view of the μSTAMPS. The labels are arranged in order of how the thruster is assembled. The thruster housing, 'a', is anticipated to be 3D printed using a space-grade polymer, such as PEEK (polyetheretherketone). The housing for the prototype was 3D printed from PETG (Polyethylene Terephthalate Glycol) for ease of use and availability.

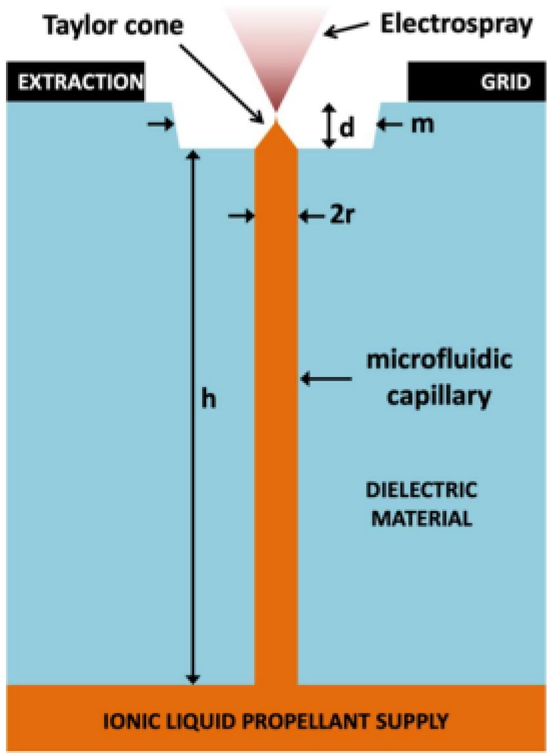

Figure 1.3: Schematic of a single capillary on the µSTAMPS emitter chip. [13]

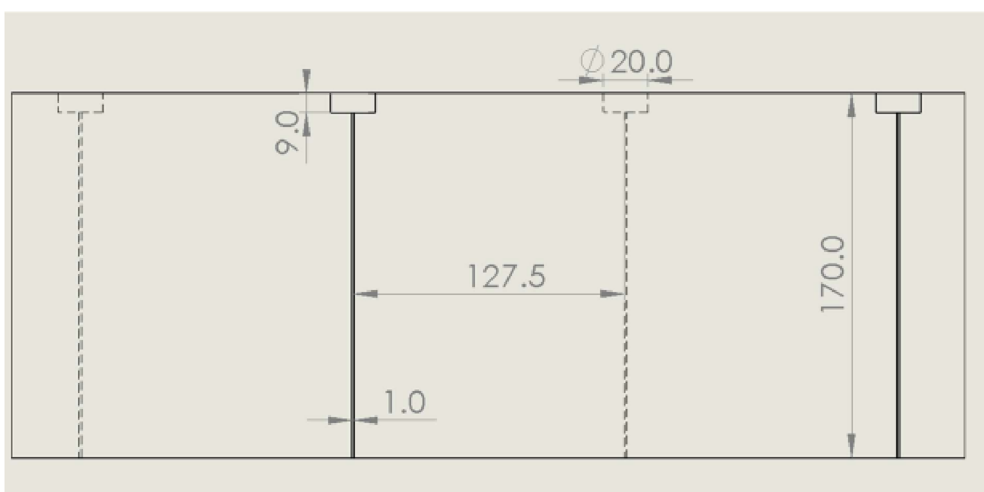

Figure 1.4: 2D drawing depicting target dimensions (in μm) of multiple capillaries on the µSTAMPS emitter chip.

A spring, labeled ‘b’, is used to press the emitter chip and porous disc reservoir together to maintain adequate hydraulic contact for capillary action to occur. The porous disc (from GM Quartz part n. 6610-037), ‘c’, is the propellant storage disc, which is placed on top of the spring. It has a 15 mm diameter, 2.5 mm thickness, and is porosity grade F, indicating that the pores are between 4 and 5.5 μm. The glass disc was determined to hold approximately 0.2 grams of propellant. While this amount of propellant is sufficient to perform limited number of collision avoidance maneuvers for certain satellites, it is not enough to deorbit small satellites from even low orbital altitudes. An external propellant tank and delivery system is therefore under development at UTSI to increase the use-case of the μSTAMPS. A piece of absorption filter paper, ‘d’, which is an intermediate 5 μm pore size Polyester PETE membrane filter (Sterlitech PET5025100), is layered over the porous disc to facilitate capillary action between the porous disc and the emitter chip by acting as a softer, flexible membrane which extends the capillary pressure gradient between the porous disc and emitter chip. The μSTAMPS emitter chip containing the array of microcapillaries and ITO coating, labeled ‘e’, is placed over the filter paper. A set of conductive bus bars are deposited on top of the coating (SPI supplies, part 06481B-AB), shown in ‘f’. A 3D printed compression frame, ‘g’, also prototyped with PETG, compresses the emitter chip and propellant storage disc with the help of the spring. The assembly is held together by a cover that is screwed into the housing, ‘h’.

A fully assembled prototype of μSTAMPS thruster is shown in Figure 1.6. The dry mass of the prototype is approximately 7.68 g. The assembled dimensions of the prototype are 30 mm $\times$ 30 mm $\times$ 8.53. Capillaries can be machined in arrays of hundreds or thousands to achieve a desired thrust level. The current design includes an emitter chip consisting of 1,203 capillaries in a hexagonal close-packed array that spans an area of 8.16 times 7.95 mm. With this configuration, the thrust is estimated to be between 1.2 μN and 12 μN with a specific impulse of at least 2,000 seconds.

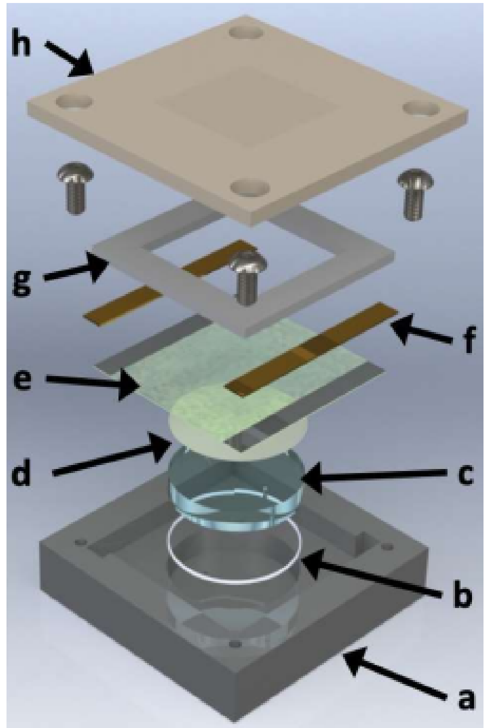

Figure 1.5: Exploded CAD view of the μSTAMPS thruster.

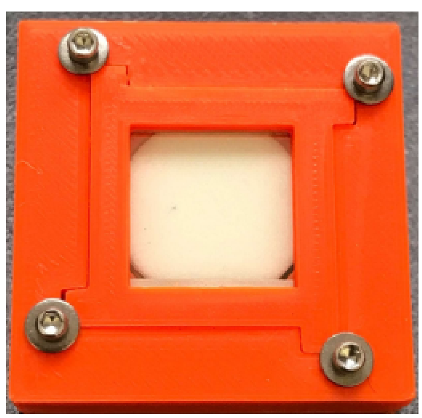

Figure 1.6: Fully assembled μSTAMPS prototype. [13]

1.3 Literature Review

Due to the increasing usage of nanosatellites, more and more electrospray thruster devices are being designed and tested. With the minuscule forces often expected from these thrusters, the thrust stands and testing methods can get complex quickly. The issues with current thrust measurement techniques for nanosatellites are largely in the balance between a simplistic design and sufficiently high sensitivity to resolve the roughly microscale forces produced by a given thruster. The test methods for these thrusters have typically been based on pendulums, either hanging or inverted, or approaches based on the principles of a torsional balance. All three of these methods are a variation of a spring-mass-damper system that allows for the precise measurement of the small thrust levels typically associated with electrospray devices, but do not come without drawbacks.

Pendulum-based thrust stands have a proven track record of accurately measuring thrust from electric propulsion devices [19],[22]. Hanging pendulums consist of a vertical pendulum arm attached to a top pivot or flexure with a thruster platform at the bottom [15]. Hanging pendulums are generally the most simplistic type of thrust stand conceptually, but the sensitivity of this approach is largely dependent on the length of the pendulum arm [15]. This means that to measure forces in the μN-range, the pendulum arm must be relatively long, up to a few meters [16]. Small vacuum test chambers are therefore insufficient for hanging-pendulum thrust stands with long pendulum arms, so these are usually the least sensitive type of thrust stands for micropropulsion.

For example, Cesare et al. [19] designed a test stand to measure thrust in the range of 1 mN for use in a cylindrical vacuum testing chamber that measures 1.2 m times 2.5 m. This system consists of two beryllium copper plates that hang from flexible mounts on a block of low thermal-expansion material. The thruster being tested is attached to one of these plates, and a counterweight on the other. The displacement of the plates relative to each other is measured as a thrust response.

Two electromagnetic actuators that produce a variable force are used to calibrate the system in situ. The stand is subject to zero drift, as all pendulum-based stands are, meaning that the zero reading is skewed by a change in the ambient conditions. This drift is caused by changes in the inclination due to thermal effects and slight structure shifts that can occur during vacuum chamber pump-down, and therefore incorporates a piezo-actuator to level the stand based on information from a high precision inclinometer.

Inverted pendulums can be used when a higher sensitivity is required. Inverted pendulums consist of a vertical pendulum arm attached to a bottom pivot or flexure with a thruster platform at the top [15]. Xu and Walker [22] discuss an inverted pendulum thrust stand, shown in Figure 1.7, measuring thrust in the range between 1 mN and 5 N. The top plate, on which a thruster mount is located, is maintained horizontally by two side plates. Thrust can be determined by the current flow of the null signal or from displacement data from a linear variable differential transformer. The sensitivity of inverted pendulums is highly dependent on flexural stiffness, which is affected by thermal changes. This necessitates thermal isolation between the thruster and thrust stand.

As discussed, hanging and inverted type pendulum thrust stands require the use of many external sensors and equipment, require careful inclination control, thermal isolation from the thruster being tested, and large facilities. Even with the inherent complexities, these thrust stands are often still not sensitive enough to measure thrust levels in the μN range [19],[22].

A torsion balance utilizes the principle of static electric force. To illustrate this concept, consider two similarly charged objects that will repel each other. When one of these objects is attached to a string, the object will twist on that string as it tries to repel the other. A light beam reflecting off a flat mirror and onto a graduated scale measures the amount of twist, and therefore, the electrostatic force between the two objects.

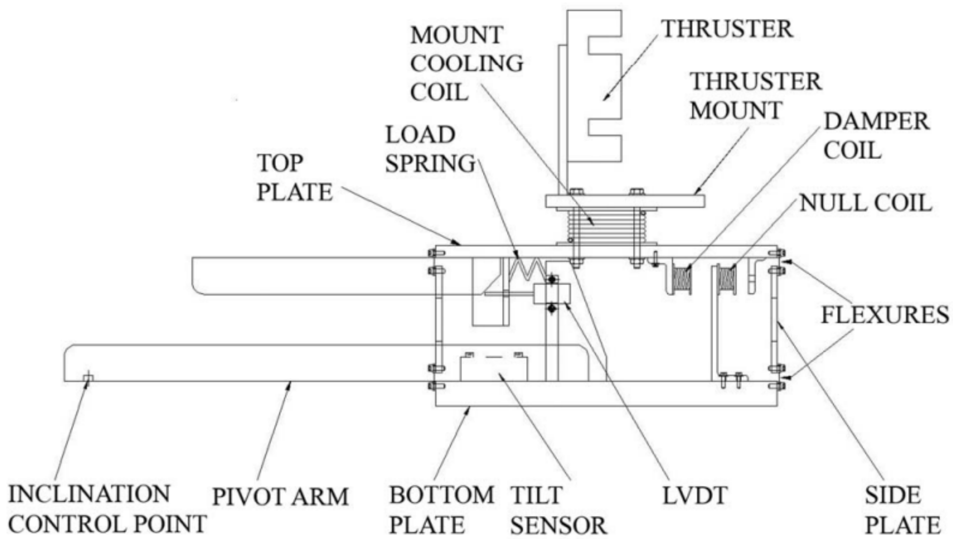

Figure 1.7: Xu and Walker's inverted pendulum thrust stand. [22]

Torsional balance methods are extremely sensitive, making them an excellent option for measuring thrust levels in the μN and even nN range, however, they are difficult to design, fabricate, and calibrate, and are often quite costly. Gamero-Castano [11] discussed a torsional balance approach capable of measuring forces in the μN range, demonstrated by firing a colloid thruster and measuring between 2 and 15 μN, and a micro-pulsed plasma thruster yielding 19 μN. This method proved to be highly accurate, with a resolution of 0.03 μN.

The set-up includes an aluminum frame with a symmetric cross beam, of which the inclination is adjusted with two stepper motors. A counterweight is incorporated on one side to balance the weight of the thruster. The arm rotates about two flexural pivots that are attached to the arm and the frame as the thruster is fired. A fiber optic displacement sensor measures the linear displacement from the axis of rotation that results from firing the thruster and is calibrated in situ [11].

A set of two cylindrical electrodes of known geometries were used to calibrate the balance displacement, one of which was attached to the balance, and one attached to an external micrometer. The gap between the electrodes was measured and the force computed using Maxwell 2D and Maxwell 3D [6]. An active linear damper was used to reduce oscillations associated with the balance [11].

Another example from Soni and Roy [18] discussed a similar torsional balance approach. Their balance, however, features an unsymmetric cross beam, shown in Figure 1.8. A copper weight is included at the short end as a counterweight to balance the unsymmetric beam. A fiber optic linear displacement sensor again measures the displacement of the balance arm. A pair of electrodes are also used to provide a known force for calibration.

The biggest difference between these two torsional-based thrust stands lies in the damping mechanism. Gamero-Castano [11] uses an active electrostatic damping mechanism, while Soni and Roy [18] use a passive eddy current mechanism. As the crossbeam oscillates, a magnetic field is generated from eddy currents induced from the relative motion between the copper counterweight and a magnet. This generated magnetic field acts opposite to the applied magnetic field, which counteracts the force proportional to the relative motion, and the kinetic energy from the oscillations is dissipated through ohmic heating. A logarithmic decrement technique is then used to calibrate the system, which uses the ratio of amplitudes from two successive peaks of damped oscillations to calculate the natural frequency, and from there estimates a spring constant.

Both of these examples, and many others, show promising results for low-level thrust measurement with very small resolutions, but at the expense of complicated calibration and/or damping techniques that also require additional equipment. Figure 1.9 shows additional ways that thrust stand techniques in the sub-μN level of resolution calibrate, dampen, and measure displacement, as well as the resolutions achieved and lowest thrust levels measured.

1.4 Thrust Stand Design

The design for the thrust stand was based on the method of measuring thrust from a combination of mass and current data using a direct measurement approach. This approach was chosen so that the system would be simplistic in construction and easy to test a variety of thrusters on, but also be sensitive enough to resolve forces in the 1 - 100 μN range. The μSTAMPS is suspended vertically over the Wipotec Weigh Cell SX-M-FS via a custom thrust stand assembly, shown in Figure 1.10. The weigh cell is used to measure the mass of ionic matters collected that is emitted from the thruster during operation. An ion collection plate acting as a Faraday cup is attached to the top of the weigh cell and connected to a picoammeter, which is used to collect current data resulting from the collection of ions. The data are recorded in a custom LabView Virtual Instrument (VI), allowing parameters such as thrust and specific impulse can be extracted.

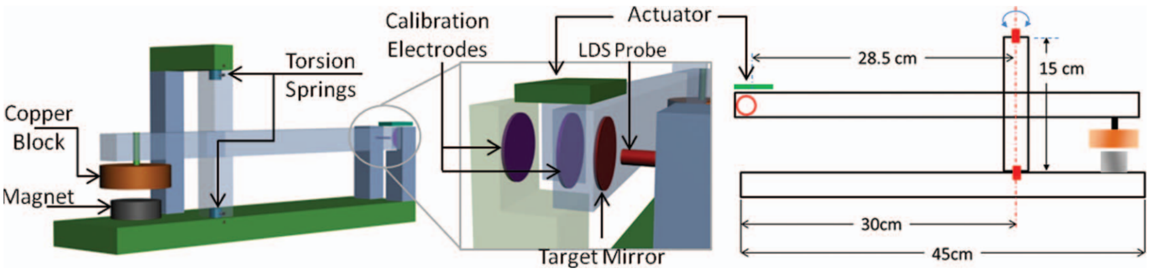

Figure 1.8: Soni and Roy torsional balance thrust stand. [18]

TABLE I. Review of thrust stands with sub-micro-Newton level resolution.

Team	Calibration source	Damping mechanism	Displacement measurement	Resolution (μN)	Lowest thrust measured (μN)
Jamison *et al.*[4]	Orifice thruster	Viscous oil bath	LVDT	<1	0.088 (±2%–16%)
Ziemer[5]	Impact pendulum	Damping coil	LVDT	<1	1.0 (±20%)
Gamero-Castaño *et al.*[6]	Electrostatic	Electrostatic	Fiber optic LDS	0.01	0.11
Gamero-Castaño[7]	Electrostatic	Electrostatic	Fiber optic LDS	0.03	7.89
Yang *et al.*[8]	Free oscillations	Air damping	Autocollimator	0.09	Not mentioned
Soni and Roy[12]	Log decrement	Eddy current	Fiber optic LDS	0.01	1.3 (±20%)

Figure 1.9: Table from Soni and Roy [18] showing calibration, damping, and displacement measurement techniques found in the literature.

The thrust stand was required to be made from low out-gassing materials for use in a vacuum chamber to optimize the testing environment. The stand was also designed to minimize environmental noise without introducing complexities into the measurement system. These requirements were accomplished by using passive damping via Viton and Teflon pads. The stack consists of a $\frac{1}{2}$ in. Viton bottom layer and a $\frac{1}{4}$ in. Teflon pad between the Viton and metal of the thrust stand. The lower stiffness of the Viton helps to eliminate higher frequency vibrations. The Teflon further adds to vibration damping as well as providing electrical isolation.

The thrust stand is machined primarily from aluminum and stainless steel stock, chosen for their vacuum compatibility and accessibility. The stand is a support structure that provides 3-axis translations to easily suspend the μSTAMPS thruster vertically above the ion collection plate on the weigh cell. The thruster is positioned with the emitters facing downward in a sliding drawer system attached to the vertical support of the stand. This drawer uses fiberglass to secure the μSTAMPS thruster mechanically as well as electrically isolate it from the rest of the system. A new fiberglass insert can be machined so that differently sized prototypes or other thrusters can be loaded and tested in a quick and inexpensive way. The completed thrust stand, designed by D'Ambro [8], is shown in Figure 1.10.

1.5 Organization

Chapter 1 established a background on the relevance of electrospray thrusters and the μSTAMPS currently under development at UTSI. It also explored the measurement techniques found in the literature. Chapter 2 will explain some governing equations involved in characterizing the performance of spacecraft and the relation to the μSTAMPS thruster. Chapter 3 will describe the set-up associated with the experiments meant to baseline the weigh cell that are imperative to accurate thrust measurements. Next, Chapter 4 describes the set-up for an experiment to determine the lowest level of thrust that is measurable with a direct approach utilizing the weigh cell. Finally, Chapter 5 will provide some key insights into the results and make recommendations for the continuation and improvement of this work.

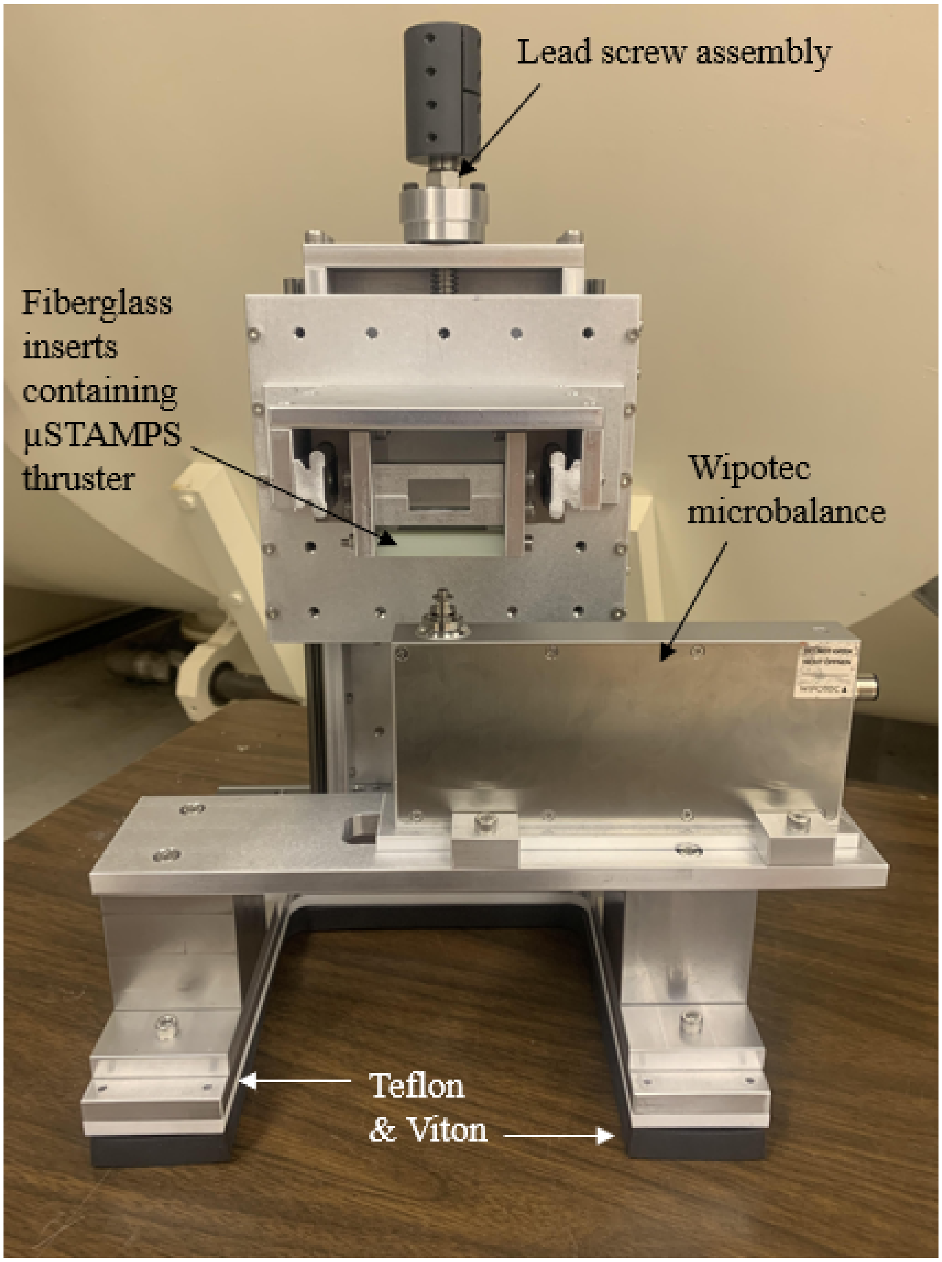

Figure 1.10: Thrust stand.

Chapter 2

Governing Equations

To appropriately characterize the performance of an electrospray device, such as the μSTAMPS thruster, some underlying background material is important to understand. Thrust, specific impulse, and efficiency are generally key parameters to analyze for any spacecraft, including electric micro-propulsion devices. Other important parameters include total velocity increment, mass fraction, and power, and especially for electric propulsion, onset voltage is also an important consideration.

Thrust is derived from Newton's second law of motion, which states the force of an object is equal to its mass multiplied by its acceleration, or mathematically [9]

$$F = ma, \tag{2.1}$$

where F is the force, m is the mass of the object, and a is the acceleration of the object.

Momentum is defined as mass multiplied by velocity, and due to the conservation of momentum and assuming no losses in the system, the time rate of change of momentum is equal to zero [9].

$$0 = \frac{m}{g_c}\frac{\Delta V}{\Delta t} - \frac{1}{g_c}v\frac{\Delta m}{\Delta t}, \tag{2.2}$$

where m is the spacecraft mass, v is the propellant exhaust velocity, t is the time, and g_c is a conversion factor , which is 1 in SI units or 32.2 $\frac{lb_m ft}{lb_f s^2}$ in English Engineering units. Taking the limit of Equation 2.2 [9]

$$0 = \frac{1}{g_c} \lim_{t \to 0} (m \frac{\Delta V}{\Delta t} - v \frac{\Delta m}{\Delta t}), \tag{2.3}$$

yields

$$0 = \frac{m}{g_c} \frac{dV}{dt} - \frac{1}{g_c} v \frac{dm}{dt}, \tag{2.4}$$

where $\frac{dv}{dt}$ is the acceleration and $\frac{dm}{dt}$ is the propellant mass flow rate, $\dot{m}$. This equation can therefore be simplified to [9]

$$F_{mom} = \frac{ma}{g_c} = \frac{\dot{m}v}{g_c}. \tag{2.5}$$

The force due to the pressure of the propellant exhaust also contributes to the total force as shown [9]:

$$F_{press} = (P_e - P_\infty) A_e, \tag{2.6}$$

where P_e is the exit pressure, P_∞ is the environmental pressure, and A_e is the exit area.

The total thrust is defined as the sum of the forces from the propellant momentum transfer and propellant exit pressure [9].

$$T_t = F_{mom} + F_{press} = \frac{\dot{m} v_e}{g_c} + P_e A_e, \tag{2.7}$$

where T_t is the total thrust, F_{mom} and F_{press} are the momentum and pressure forces respectively, $\dot{m}$ is the propellant mass flow rate, v_e is the propellant exit velocity, g_c is the gravity unit conversion factor, P_e is the propellant exit pressure, and A_e is the exit area.

Recognizing that the thruster will be operating in space and has no pressure differential with vacuum allows Equation 2.7 to be simplified [9]

$$T_t = \frac{\dot{m} v_e}{g_c}. \tag{2.8}$$

The mass flow rate, $\dot{m}$, can be calculated from experimental results of electrospray devices by using the equation [7]

$$\dot{m} = I_{ion} \times \frac{m_{ion}}{q_{ion}}, \tag{2.9}$$

where I_{ion} is the ion current, m_{ion} is the mass of the ions, and q_{ion} is the ion charge.

The total impulse is the average thrust over the total firing time and is proportional to the total amount of energy released by the propellant. This can be shown mathematically by integrating the total thrust equation over the firing time of the thruster, as shown [20]:

$$I_t = \int_{t_0}^{t_f} T_t \, dt, \tag{2.10}$$

where I_t is the total impulse, t_0 is the starting time of thrust, and t_f is the final time of thrust.

Total impulse can be used to determine the specific impulse, defined as the total impulse per unit weight of propellant [20]. This parameter is used frequently in propulsion systems to denote how efficiently propellant is being used. It is measured in seconds, indicating how long one kilogram of propellant can produce one newton of force [9]. Specific impulse can thus be obtained by dividing Equation 2.10 by the mass expelled during the time of thrust, or

$$I_{sp} = \frac{\int_{t_0}^{t_f} T_t \, dt}{g_c \int \dot{m} \, dt}, \tag{2.11}$$

where I_{sp} is the specific impulse.

Equation 2.11 accounts for thrust that varies with time, such as during start-up and shutdown of the thruster. During periods of constant thrust, this equation can be simplified as [20]

$$I_{sp} = \frac{I_t}{m_p g_c}, \tag{2.12}$$

where m_p is the total effective propellant mass ejected from the thruster.

Equation 2.11 can also be written as follows when the propellant mass flow rate is constant, the thrust produced is constant, and when the start and stop transients are negligibly short: [20].

$$I_{sp} = \frac{v_e}{g_c}. \tag{2.13}$$

The equation can also be expressed [20] in its most common form:

$$I_{sp} = \frac{T_t}{\dot{m} g_c}. \tag{2.14}$$

Equation 2.4 can thus be rewritten using Equation 2.14 [9]:

$$0 = m\frac{dv}{dt} + g_c I_{sp}\frac{dm}{dt}. \tag{2.15}$$

Rearranging and integrating results in an equation for the maximum velocity increment achievable for a given mass fraction and specific impulse [9]:

$$-g_c I_{sp} \int_{m_0}^{m_f} \frac{dm}{m} = \int_0^{v_f} dv, \tag{2.16}$$

$$\Delta v = -g_c I_{sp} ln(\frac{m_f}{m_0}), \tag{2.17}$$

where Δv is the total velocity increment available, m_f is the vehicle dry mass and m_0 is the vehicle dry mass plus the mass of the propellant. The ratio of these two values, $\frac{m_f}{m_0}$, is known as the mass fraction, f_m [9]. Equation 2.17 is known as the rocket equation.

Thrust power can be determined from I_{sp} using Equation 2.18 [9]:

$$Q = \frac{1}{2}\dot{m}v_e^2 = \frac{1}{2}\dot{m}g_c^2 I_{sp}^2, \tag{2.18}$$

where Q is the thrust power.

Additionally, thrust power per unit area can be determined from [7]

$$\frac{Q}{A} = \frac{\dot{m}v_e^2}{2A}, \tag{2.19}$$

where A is the thrust area, the active area, i.e. the emitting area of the emitter chip, for example.

The efficiency can also be determined using Equation 2.20 [20]:

$$\eta = \frac{\frac{2v}{v_e}}{1 + (\frac{v}{v_e})^2}. \tag{2.20}$$

These equations show how thrust can be calculated when parameters such as propellant mass flow rate and exit velocity are known, or can be calculated, but they also show how various other performance parameters can be determined if the thrust is known. Equations 2.8 through 2.14 show how thrust is used to calculate specific impulse, which is an important parameter to analyze for spacecraft, especially when determining how much propellant is required to achieve specific missions.

Chapter 3

Experimental Set-up and Baseline Experiments

This chapter will focus on the set-up for the experiments conducted to baseline the testing equipment, the results of each test, and the implications on the minimum thrust measurement.

3.1 Equipment

The goal is to determine if a direct measurement approach is suitable for the characterization of the μSTAMPS, or μN-range thrusters in general, while avoiding the complex set-up, damping, and calibration requirements of traditional direct measurement thrust stands [11], [18]. At the center of this direct-measurement approach is the idea of using an ultra-sensitive mass balance, capable of resolving the expected forces. The Wipotec Weigh Cell model SX-M-FS was selected, as its 20 μg resolution would theoretically be able to resolve forces of approximately 0.2 μN [1]. The weigh cell also has a single impingement point with a 10 g measuring range and a fast settling time of 220 ms [1]. Experiments were conducted to determine if this weigh cell matches the manufacturer's specifications and ultimately, to determine the true lower limit of thrust that can be measured.

3.1.1 Equipment Set-up

The Wipotec weigh cell is powered by a 24 V programmable power supply (BK Precision, model: 1787B) set to 24 V and up to 1 A maximum current output, and the weigh cell controller is powered from a custom power supply providing −24 V. The programmable and controller power supplies share a common ground. The weigh cell is connected to a computer via an RS-232 cable for data collection. Connection to and operation of the Wipotec balance can first be verified by running the simple interface program supplied by Wipotec. For measurements, a custom LabVIEW Virtual Instrument (VI) is used to collect mass data over time from the weigh cell at a adjustable sampling rate. After appropriately wiring the Wipotec, the weigh cell must "warm up" to the ambient conditions and stabilize , which is indicated by the appearance of the unit symbol following the mass measurement value in the Wipotec-supplied interface program.

3.2 Baseline Experiments

Before the testing of the thruster could be conducted, measures were taken to ensure that the equipment selected to collect data operated as intended and was sufficiently sensitive for the expected measurements. The Wipotec Weigh Cell is the focus of these baseline experiments. Characterizing the performance of the weigh cell is important to determine what noise is present and work to isolate or account for it. Developing a baseline also ensures that when thrust data is collected, there is confidence that the data is a true representation of the thruster performance.

3.2.1 Mass Calibration

The mass under test must be evaluated to determine if the measurements obtained are correct, and if they are not correct, by how much. This is imperative to determine accurate thrust levels, especially on the level of μN, where high resolution is required. The weigh cell was checked to see if the mass measurements obtained aligned with expected values by using a set of calibration weights. The calibration weights were weighed on a calibrated precision balance to ensure they matched the specified mass value. A UHAUS Pioneer Precision Digital Balance was used to check the values of the calibration weights because it has a resolution of 0.1 mg and features an enclosed weighing pan to shield the measurement from air currents.

The Wipotec was set-up as described in Section 3.1.1. The calibration weights were then placed individually on the weigh cell to compare and evaluate differences. Table 3.1 shows the expected mass value of each calibrated weight, the mass reading obtained from the Wipotec weigh cell and Pioneer digital balance, and the differences between the expected and actual values for each. The 500 mg and 2,000 mg calibration weights had duplicates and each were tested.

Figure 3.1 shows the difference in milligrams between the calibration weights and the values obtained from each balance. The digital balance was closer to the expected value of the calibration weights than was the Wipotec weigh cell by a very slim margin. This is likely due to the enclosed weighing pan on the digital balance, which restricts air drafts that may affect measurement readings. The Wipotec weigh cell was not enclosed for the measurements. This small discrepancy should not be a considerable factor for thrust measurements taken in future tests, as they will be conducted in a vacuum chamber, where air drafts can be eliminated entirely. An outlier to these data is noted in the first 2,000 mg row, where the percent error is 1.1061% for the Wipotec weigh cell and 0.9041% for the precision balance, calculated using Equation 3.1 below.

Table 3.1: Calibration weight masses in mg recorded by the Wipotec weigh cell and Pioneer digital balance, and % differences with the expected values.

Expected	Wipotec	% Difference	Digital	% Difference
500	499	0.2002	500	0.0000
500	502	−0.3992	503	−0.5982
1000	998	0.2002	1000	0.0000
2000	1978	1.1061	1982	0.9041
2000	1992	0.4008	1996	0.2002
5000	4990	0.2002	5000	0.0000

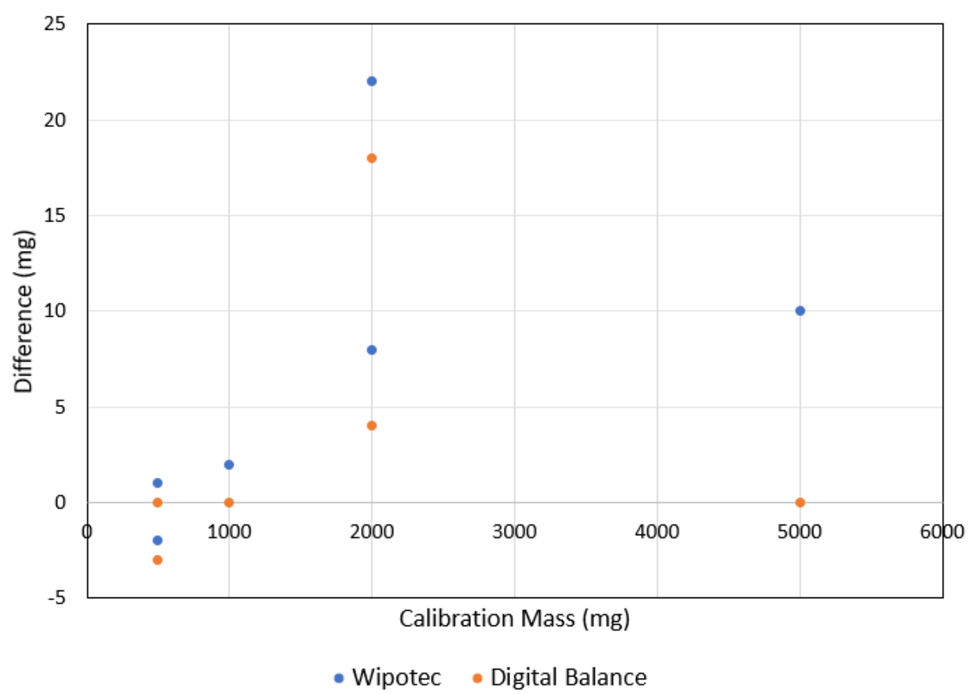

Figure 3.1: Measurement differences between the Wipotec weigh cell and Pioneer digital balance for calibration weights.

Since the error is much higher than all other calibration weights for both measurement methods, the calibration weight was assumed to be damaged, resulting in the lower mass, and the measurements disregarded. The calibration weights available were too large to calibrate the lower limit of the Wipotec weigh cell, but the error percentages do not seem to propagate as the order of magnitude increases or decreases, so few issues are anticipated regarding this. This test validates the mass measurement ability of the Wipotec weigh cell for the range tested.

$$\% \quad \text{difference} = \frac{\text{calibration} \quad \text{mass} - \text{measured} \quad \text{mass}}{\frac{1}{2}(\text{calibration} \quad \text{mass} + \text{measured} \quad \text{mass})} \quad \times \quad 100\% \tag{3.1}$$

3.2.2 Settling Time

The next baseline experiment to be conducted was to determine if the settling time of the Wipotec Weigh Cell corresponded to the manufacturer's claim of 220 ms. A contact angle test machine (Kruss, DSA100) was used to evaluate this performance because it allows for small, known volumes of liquid to be dispensed from a syringe, which was important to simultaneously determine if the theoretically expected force matched the measured force. This machine is typically used to measure the contact angle of a liquid on a certain surface to know the wettability of the surface, but it was able to be utilized for this baseline experiment because the volume of liquid dispensed was known, and sufficiently small for use on the weigh cell. The weigh cell was placed in-line with the camera of the contact angle machine. The syringe was filled with deionized water and positioned directly above the impingement point of the weigh cell.

The Wipotec was set up as described in Section 3.1.1. The weigh cell was allowed approximately two hours to warm up. Foam rubber padding was placed between the weigh cell and testing surface to help dampen building vibrations, and cardboard sheet baffles were arranged surrounding the weigh cell to reduce the effect of air drafts for more consistent measurements. The distance from the syringe to the collection plate on the balance was measured and recorded. Once the balance was fully stabilized, the contact angle machine was set to drop a 9 μL droplet of DI water onto the impingement point of the balance. The balance was allowed time to settle, and same size droplets were dropped several more times for comparison. The test was repeated with 10 and 12 μL droplets. Figure 3.2 shows an example of the mass readings that were recorded during a typical 9 μL droplet experiment.

The settling time was determined by subtracting the time when the droplet was first registered by the weigh cell from the time the balance fully settled and reached equilibrium again. The average settling time for the set of tests from each droplet size is shown in Table 3.2. For the 9, 10, and 12 μL droplets, 12, 13, and 4 values were collected and averaged, respectively. The average settling time across all tests was 226 ms, which corresponds well to the manufacturer's statement of 220 ms.

The force imparted on the balance by the droplets was also obtained by applying basic physical mechanics and kinematic equations. Comparing theoretical data to experimental data further validates the measurements taken.

The droplet mass can be calculated from

$$m = \rho V, \tag{3.2}$$

where m is the mass of the droplet, ρ is the density of the water, and V is the volume of water in the droplet. The final velocity of the droplet, assuming zero initial velocity because the droplet starts falling from rest, is calculated from the kinematic equation

$$v_f = \sqrt{2gh}, \tag{3.3}$$

where v_f is the velocity of the droplet upon impact, g is the gravitational constant of 9.81 $\frac{m}{s^2}$, and h is the height above the collection plate from which the droplet was dropped.

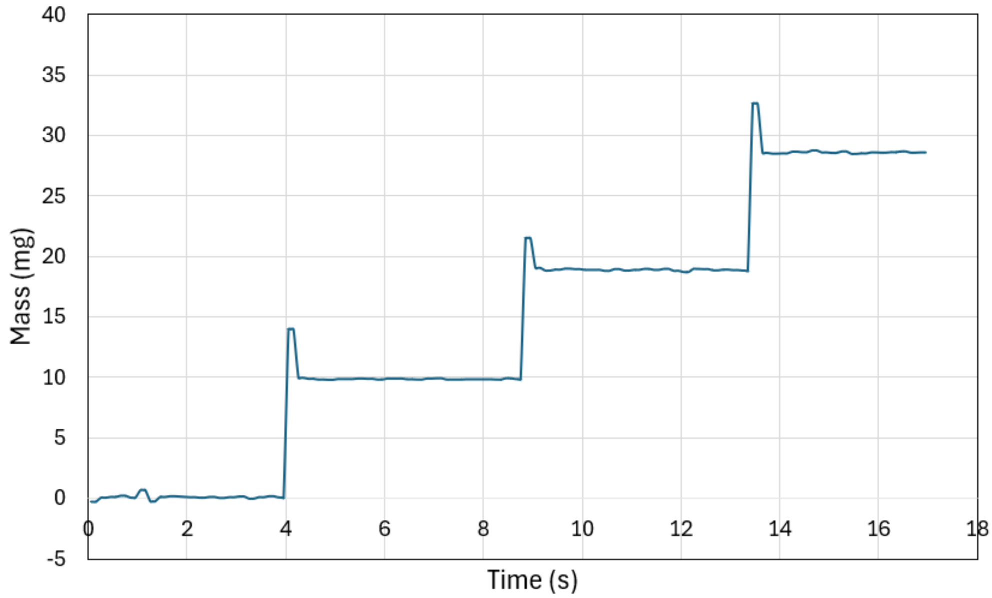

Figure 3.2: Settle time experiment with 9 μL droplets.

Table 3.2: Average settling times for 9, 10, & 12 μL droplets in ms.

	9 μL	**10 μL**	**12 μL**	**Average**
Average	249	216	215	226

The momentum can be calculated using

$$p = mv_f, \tag{3.4}$$

where p is the final momentum the droplet has as it contacts the collection plate (again assuming the droplet starts from rest).

The force imparted on the balance can then be determined from Newton's Second Law using the form

$$F = \frac{\Delta p}{\Delta t}, \tag{3.5}$$

where F is the force imparted upon the balance from the droplet falling, Δp is the change in momentum and Δt is the change in time. Assuming there is no initial momentum associated with the drop and Δt is the time for the droplet to come to rest after it contacts the collection pan, Equation 3.5 simplifies to

$$F = \frac{p}{t}, \tag{3.6}$$

where p can be determined from Equations 3.4 and an estimate for t can be estimated from the time between when the Wipotec first registers a force and the top of the peak created by the force.

The force imparted from the 9 μL droplet was determined to be 71.3 μN, the force from the 10 μL droplet was 118.4 μN, and the force from the 12 μL droplet was 129.2 μN. These values are an upper estimate since the accuracy of the time estimate required to utilize Equation 3.6 is limited to the sampling rate of the LabVIEW VI that is collecting the data. The calculated values obtained align relatively well to the measured values, within an order of magnitude.

3.2.3 Electrical Resistance Experiment

Another baseline experiment was conducted to determine if the presence of an electrical current had an impact on the read-out of the balance. This was important to determine if the ionic charge transfer, i.e. current, during the thrust measurement would affect the weigh cell read-out, since the weigh cell chassis is in electrical series to ground. To evaluate this, a voltage was stepped up from 0 V to 100 V in regular increments of 10 V and the voltage, current, and mass data were recorded. The polarity was then reversed, and the experiment was repeated to check for any variation due to current polarity, since the μSTAMPS thruster is designed to emit ions of both polarity during normal operation.

For this experiment, the weigh cell was placed in the vacuum chamber on the thrust stand, discussed in Section 1.4, to eliminate air currents from disrupting the data. The Wipotec weigh cell was set up as described in Section 3.1.1 and allowed to warm up for approximately one hour. A nylon washer was placed in between the weigh cell and the stainless-steel collection plate to electrically isolate the balance measurement portion of the device from the weigh cell chassis. A drop of conductive ionic liquid, EMI–BF4 (1-ethyl-3-methylimidazolium tetrafluoroborate), was placed on the collection plate and two metal wires were inserted into the liquid drop. One wire was connected to a high-voltage power supply (Stanford Research Systems model: PS310/1250V) in series with a 5 GΩ resister box, resulting in an applied current of 2×10^{-9} to 2×10^{-8} amps as the voltage was stepped from 10 V to 100 V, which is representative of the current level expected from the μSTAMPS when operating. The other wire placed in the liquid was connected to a picoammeter (Keithely 6485) to collect current data. The instruments and data collection were again controlled through custom LabVIEW VIs, although in this case, the VI controlling the voltage and current was run independently of the weigh cell VI. A schematic showing the wiring for this experiment is shown in Figure 3.3 and the actual set-up inside the vacuum chamber is shown in Figure 3.4.

As shown in Figures 3.5 and 3.6, the mass readings increased over time for both the positive and negative polarities.

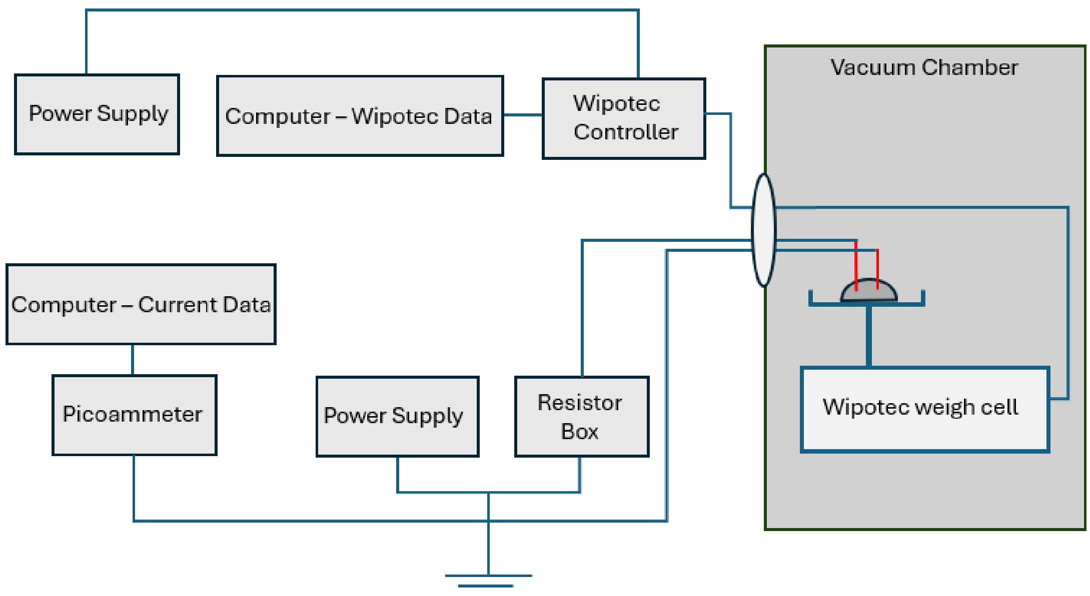

Figure 3.3: Resistance experiment schematic.

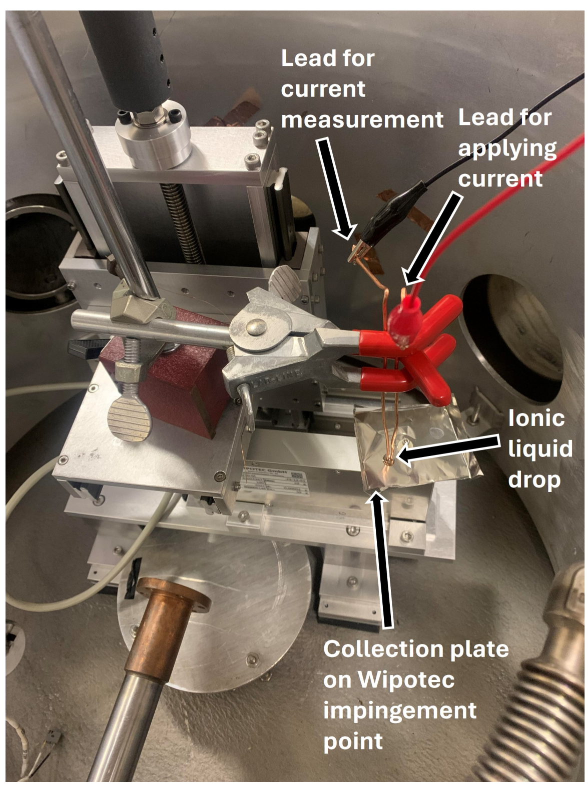

Figure 3.4: Resistance experiment set-up inside vacuum chamber.

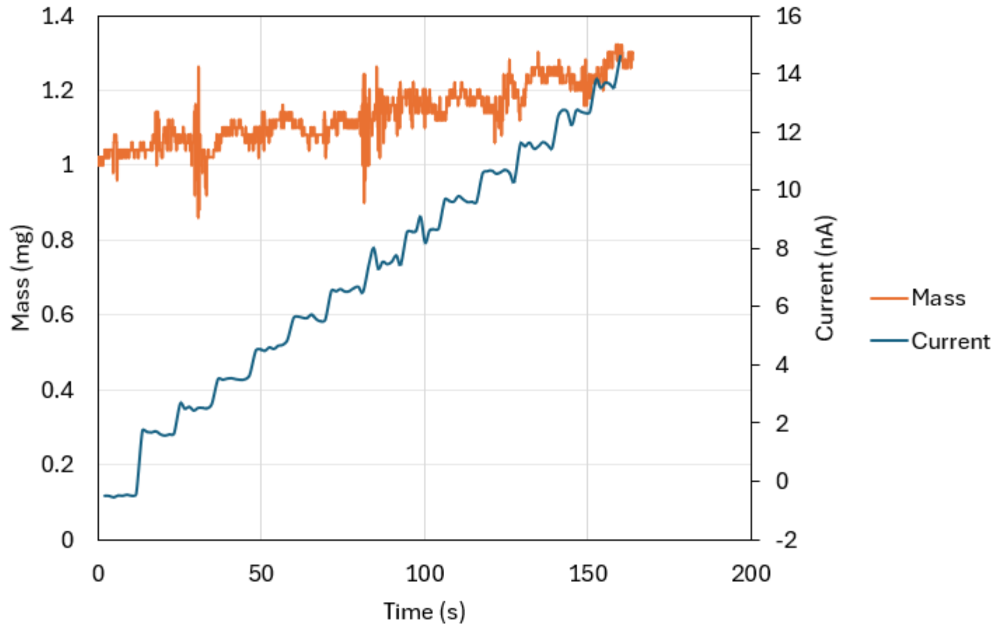

Figure 3.5: Positive polarity voltage stepped by 10 V.

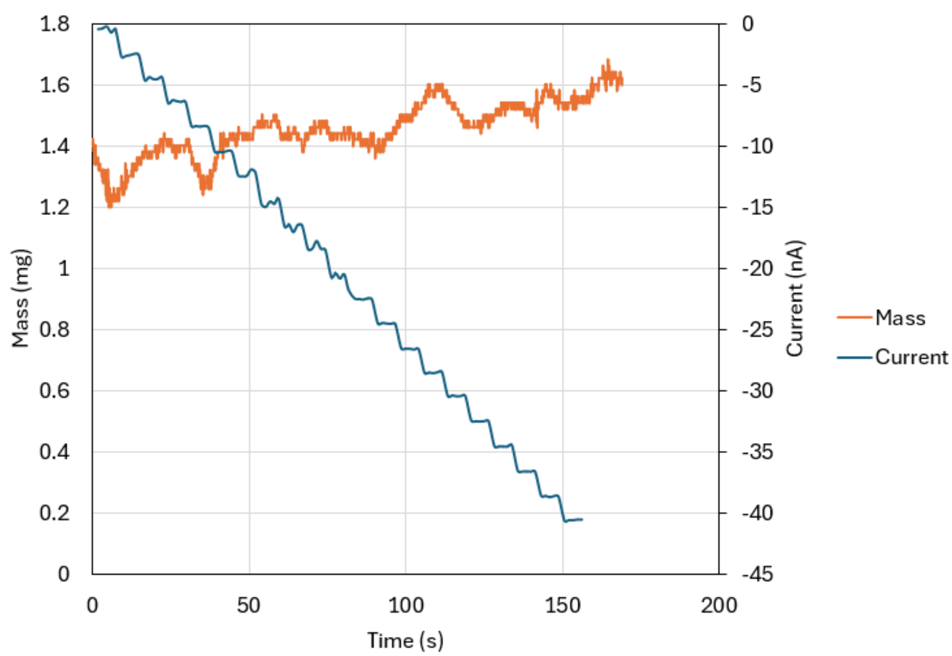

Figure 3.6: Negative polarity voltage stepped by 10 V.

This experiment was conducted again to determine if the cause of the increase was due to the voltage being applied or if there was a drift associated with the weigh cell. When the experiment was conducted again, the LabVIEW VI was set to begin collecting data without any voltage applied check for bias in the weigh cell measurement. The obtained data yielded a slope that could be fitted and then filtered out of the data, shown in Figure 3.7. The picoammeter was not included again on the next iteration to simplify the set-up, as the current values were already verified from the first measurement data. Once sufficient data were obtained for the slope, the voltage was applied, stepping again from 1 V to 100 V in increments of 10 V.

With the slope from the case with no applied voltage subtracted from the data, it is easy to see from Figure 3.8 that there is almost no change in reading resulting from the applied voltage. There appears to be no correlation between applied currents of the magnitude expected from the μSTAMPS operation and change in the reading from the Wipotec weigh cell. The change noted in the first case was likely due to an insufficient warm-up time. To combat this issue in future experiments, the weigh cell should be powered on and allowed to warm-up overnight, or at least for many hours.

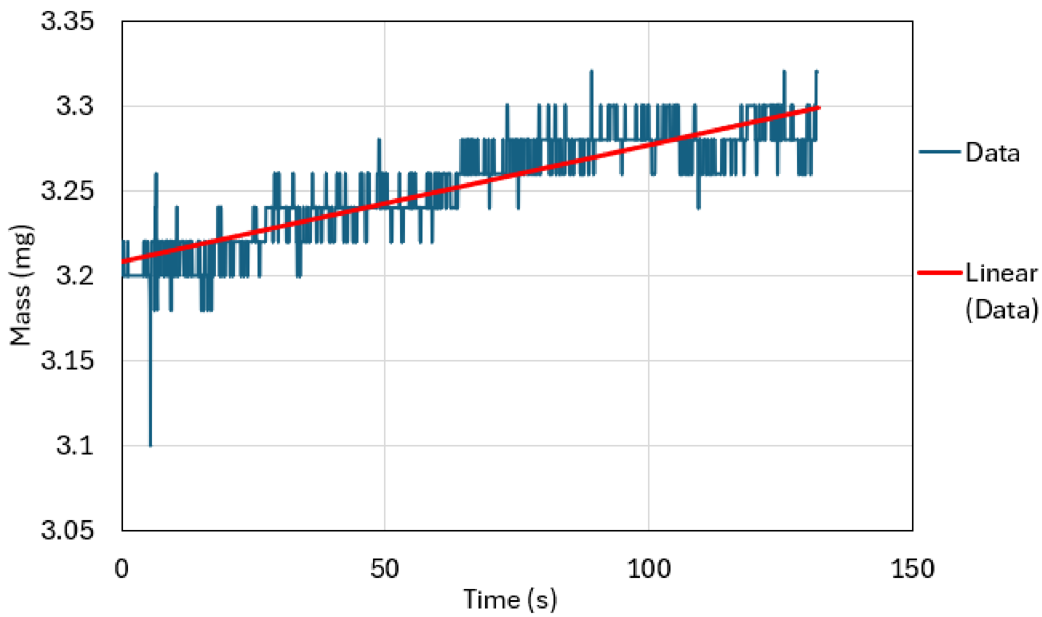

Figure 3.7: Data collected as a baseline to determine the slope over several minutes.

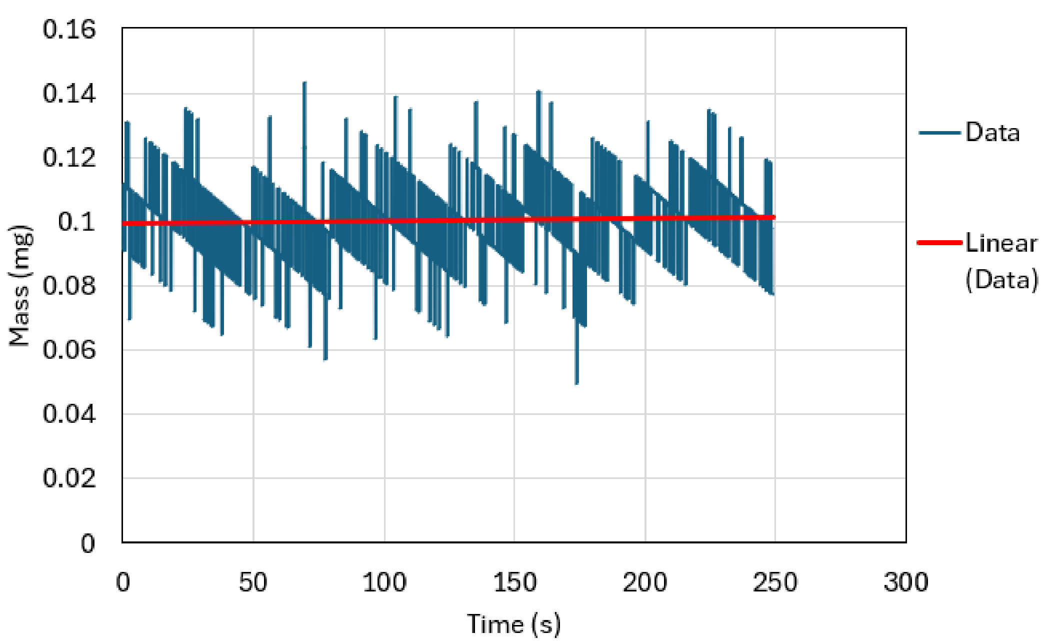

Figure 3.8: Data with the slope filtered out to show true trend.

Chapter 4

Minimum Thrust Experiments: Results and Discussion

4.1 Minimum Thrust Level Experimental Set-up

After all the baseline experiments were completed to ensure the testing equipment operates as intended with the same sensitivity as expected, an experiment to determine the minimum measurable thrust was completed. The goal of this experiment was to determine the minimum thrust level that the μSTAMPS thruster would need to produce to be measured with the designed thrust stand and a direct-measurement approach. This information is valuable as prototyping begins, since the number of capillaries that need to be machined can be calculated from an estimate of the thrust produced from each capillary. This would reduce the need to resize and re-machine the emitter chip and/or housing assembly. The thrust is important to be measurable and accurate to ensure the μSTAMPS will achieve the mission requirements for a given satellite and determine how many thrusters should be included on the satellite to meet those requirements. The minimum measurable thrust level from this experiment will determine how much thrust is required from a single thruster to be accurately measured.

The methodology for this experiment was to drop known masses onto the weigh cell in decreasing size to determine the minimum force measurable by the weigh cell. The object is required to be small enough to create a minimum level of force, and to be either precision-machined to a known mass, or for the mass to be determined with a reasonable level of accuracy and repeatability. One method that was attempted included using the Drummond Nanoject II nano-injector (Model 3-000-204/205A/206A) to drop a precision droplet of water onto the weight cell. Since the equipment that was readily available was a nano-injector rather than a dropper, the largest selectable single volume (69 nL) would not drop. It would instead collect on the tip of the injector capillary because of surface tension and capillary forces. Many "injections" were necessary for the weight of the composite droplet to overcome the surface tension and separate from the capillary. The volume of water would then be too large to determine a true minimum force.

Precision-machined materials are typically expensive, so other options were considered. Individual grains of salt and sugar were proposed as potential low-cost, readily available options. A single grain of sugar was placed under a microscope (Model Olympus BX60M) at 10 times magnification. The grain's dimension in the z-direction was measured in μm using the notched scale focusing dial on the microscope, and the x-dimension and y-dimension were measured by capturing an image and using the calibrated measure tool in the imaging software, Infinity Analyze. This process was repeated for several grains, and the sugar was found to have very jagged and irregular shapes, as shown in Figure 4.1, with standard deviations of 185, 223, and 78 μm for the x-, y-, and z-directions, respectively, based on a sample size of four grains. The process was repeated again for standard iodized table salt, which was found to be much more consistent. Each grain was a cubical shape, as shown in Figure 4.2, and the dimensions were much closer in size, with standard deviations of only 51, 46, and 60 μm for the x-, y-, and z-directions, respectively, based on a sample size of six, as shown in Table 4.1. Salt was deemed acceptable for the experiment, since this deviation is far below the resolution of weigh cell.

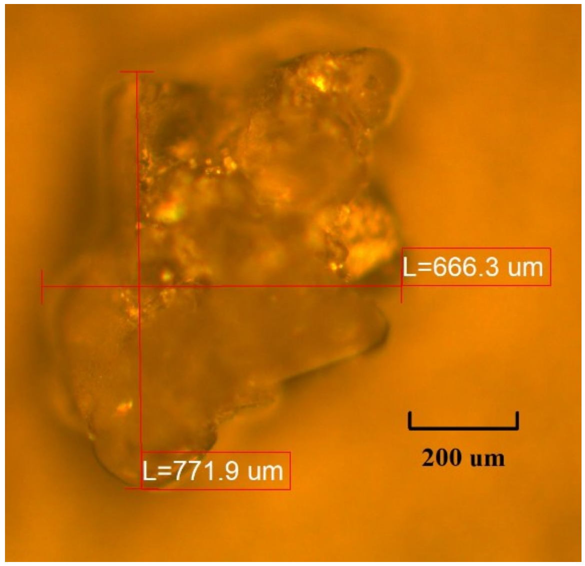

Figure 4.1: One grain of sugar at 100 times magnification.

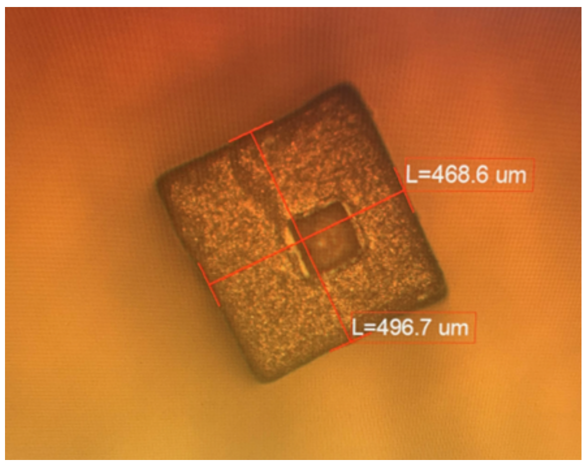

Figure 4.2: One grain of iodized salt at 100 times magnification.

Table 4.1: Dimensions in μm for six different grains of common table salt.

	1st	**2nd**	**3rd**	**4th**	**5th**	**6th**	**Average**	**Standard Deviation**
X	437	496	469	441	360	357	426	51.3
Y	460	482	497	452	403	351	440	46.0
Z	400	440	510	460	370	310	415	59.7

The density was noted to be 1.22 $\frac{\text{mg}}{\text{mm}^3}$ for iodized salt [2] and used along with the measured volume to obtain the mass for the average grain of salt of 0.0961 mg.

To conduct the experiments, the Wipotec was set up as described in Section 3.1.1 and allowed to warm up overnight. A small stainless-steel sheet was placed on the impingement point of the balance to increase the measurement surface area, allowing for easier collection of the salt grains.

Once fully settled, the weigh cell was tared, and the custom LabVIEW VI was opened for collecting data. The resolution of the weigh cell is denoted by the manufacturer to be 0.02 mg, so the lowest theoretical force the weigh cell can measure is approximately 0.2 μN. Based on this figure, the experiment was initiated with four gains of salt being dropped simultaneously. This was conducted a total of four times and the mass data from the weigh cell of each drop was recorded. Each time the experiment was conducted again, the same four grains of salt were used to minimize uncertainty in the data during post-processing. The process was repeated for a collection of two grains dropped simultaneously, then a single larger grain, and finally a single smaller grain.

4.2 Results

The mass measurements were recorded in LabVIEW, and the raw data were imported into MATLAB for processing. The data were smoothed using a Savitzky-Golay filter, which is a moving filter that smooths based on least-squares fitting of the data by polynomials as it slides across the data. The smoothed data was split into two sections: the measurements just before the grains impacted the collection plate and the measurements just after the balance reached equilibrium again after the grains impacted the collection plate. The average reading was taken from each section. The initial mass average was subtracted from the final mass average to reveal the mass increase as a result of dropping the grains.

The four-grain case was evaluated first, as it was likely to be the easiest case to distinguish any differences in mass. The same four grains of salt were used for each test to determine how consistently the weigh cell was measuring the mass. All four tests were imported into MATLAB, where the mass difference was determined. Figure 4.3 shows an example of the imported data, with the drop of the grains occurring around 10 seconds. The graph also shows the need to average the equilibrium before and after the force is imparted on the impingement point, as not all the grains fell at the exact same time.

The masses measured for tests one, two, three, and four were 0.7566 mg, 0.8094 mg, 0.8025 mg, and 0.8059 mg, respectively. The resulting average is 0.7936 mg, with a standard deviation of 0.0248 mg. At a significance level of 0.05, the first test resulting in a mass difference of 0.7566 mg is an outlier and can be rejected. The new average is 0.8059 mg with a standard deviation of 0.0035 mg. Using Equation 2.1, the force can be determined.

$$F = ma = (0.8059\,\mathrm{mg})(9.81\,\frac{\mathrm{m}}{\mathrm{s}^2}) = 7.91\,\mu\mathrm{N}.$$

The force measured is 7.91 μN with a standard deviation of 0.034 μN when the mass is multiplied by the gravitational constant to obtain force. Thrust levels in this range can thus comfortably be measured with accuracy.

The four grains of salt were then weighed on another balance, the OHAUS Pioneer Precision Digital Balance, to compare the mass values. The Pioneer digital balance has a lower resolution than that of the Wipotec, at 0.1 mg. The grains were measured a total of six times, with readings between 0.0008 g and 0.001 g with an average of 0.00086 g, or 0.86 mg. Despite the lower resolution of the digital balance, the values seem to agree well within an order of magnitude.

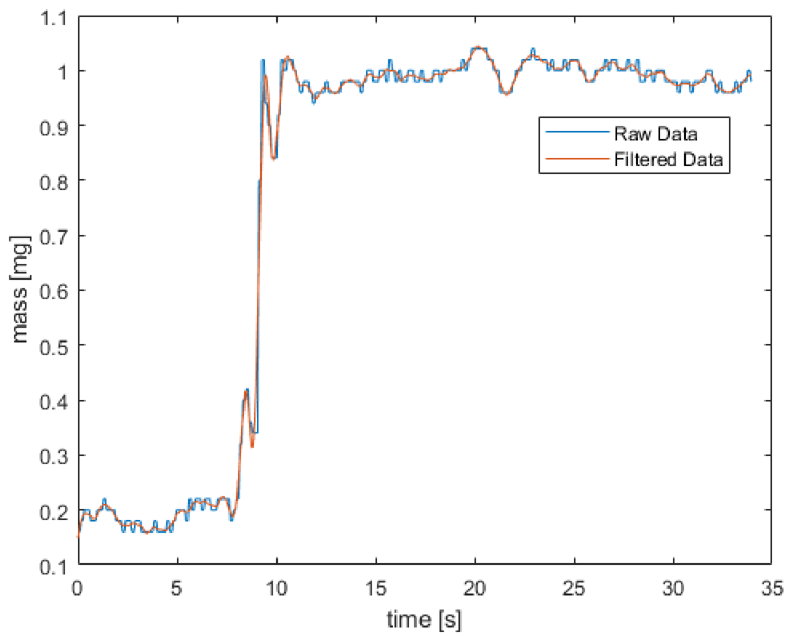

Figure 4.3: MATLAB graph showing four grains dropped simultaneously.

The mass values obtained from the precision balance and Wipotec weigh cell, however, did not agree with the mass calculated from the volume and assumed density of the grains. Each grain was placed under the microscope again and its dimensions remeasured to ensure that the correct objective was selected within the imaging software, and also to determine if the grains selected for the experiment were close to the average volume determined previously of 0.0778 mm^3. The average volume of the four grains dropped was found to be 20.69% higher at 0.0958 mm^3 due to the presence of one very large grain. This average volume multiplied by a density of 1.220 $\frac{mg}{mm^3}$ results in an average mass of 0.1168 mg for one grain and a total of 0.4670 mg for four identical grains. This calculation does not account for the total error present, however. A calibration graticule was used to ensure that the measurement tool in the imaging software agreed with the actual measurements and was found to be accurate. The four grains were once again weighed on another precision balance, a Mettler Toledo precision digital balance (Model MS104S), to further ensure the Wipotec weigh cell produced an accurate reading. The mass recorded from this third balance agreed with the Wipotec weigh cell and Pioneer precision balance. The cause of error associated with the calculated mass value is unknown but assumed to involve incorrect density data. Therefore, calculations based on volume and density will not be used to verify Wipotec weigh cell readings since the density is difficult to determine experimentally, and even the dimension measurements may be inaccurate, as the entire surface of the grain cannot be imaged at one time, and irregularities on the other faces of the cubic structure may not be visible. It was decided that the mass readings would instead be verified by the Mettler Toledo precision balance.

The same testing and post-processing procedures were repeated for two grains of salt that are approximately uniform in size but not from the original four grains selected. The drop test was conducted a total of 15 times, as shown in Table 4.2. The average mass obtained was 0.9577 mg with a standard deviation of 0.0081 mg.

Table 4.2: Mass in mg measured for two grains of iodized salt.

Test	**Mass (mg)**
1	0.9417
2	0.9558
3	0.9571
4	0.9675
5	0.9491
6	0.9567
7	0.9522
8	0.9515
9	0.9733
10	0.9577
11	0.9656
12	0.9602
13	0.9673
14	0.9572
15	0.9535
Average	0.9577
St dev.	0.0081

The force is again determined from Equation 2.1:

$$F = (0.9577\,\text{mg})(9.81\,\frac{\text{m}}{\text{s}^2}) = 9.40\,\mu\text{N}.$$

As seen in Figure 4.4, a noticeable jump is present at approximately 8 seconds, indicating a force of 9.4 μN can be identified and measured with a standard deviation of 0.08 μN. The mass from the two-grain test is larger than the mass of the four-grain test because the salt was replaced for the two- and one- grain tests and the average grain size was larger for the replaced salt. The two grains were weighed on the Mettler digital balance three times and the measurement readings were 0.0009 g, 0.0010 g, and 0.0010 g, validating the Wipotec mass reading of approximately 0.95 mg.

The same testing and post-processing procedures were repeated for one large grain of salt, selected separately from the previous tests. This test was also conducted a total of 15 times, as shown in Table 4.3. The average mass measured was 0.5088 mg with a standard deviation of 0.0109 mg. The force determined is

$$F = (0.5088\,\text{mg})(9.81\,\frac{\text{m}}{\text{s}^2}) = 4.99\,\mu\text{N}.$$

As seen in Figure 4.5, a noticeable jump is present again, indicating a force of approximately 5 μN can be identified and measured with a standard deviation of 0.11 μN. The large grain was weighed on the Mettler digital balance three times, and each measurement reading was 0.0005 g, or 0.5 mg. This value matches the mass read-out from the Wipotec.

The same testing and post-processing procedures were again repeated for one small grain of salt that was selected separately from the previous tests. The test was once more conducted a total of 15 times, as shown in Table 4.4. The average mass measured was 0.0989 mg with a standard deviation of 0.0078 mg. The force in this case is found to be

$$F = (0.0989\,\text{mg})(9.81\,\frac{\text{m}}{\text{s}^2}) = 0.97\,\mu\text{N}.$$

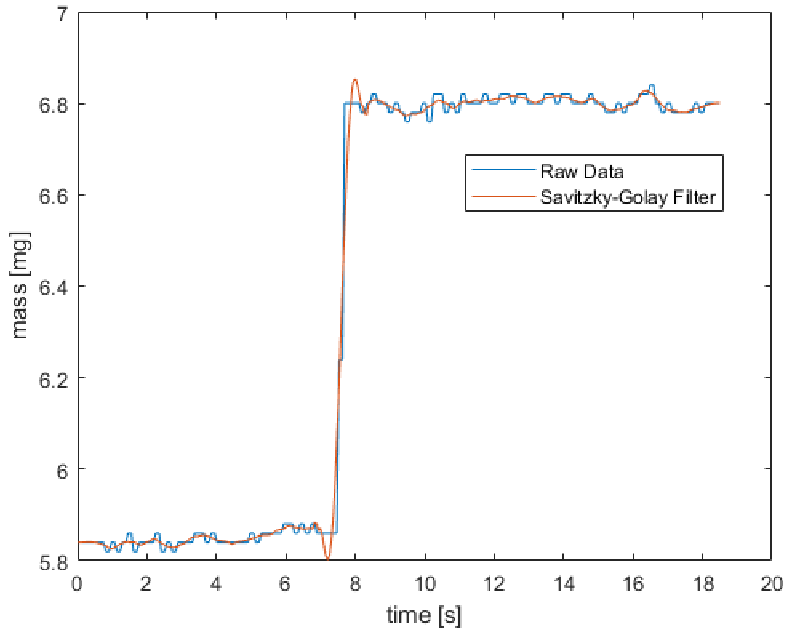

Figure 4.4: Wipotec response to two salt grains dropped simultaneously on the weigh cell.

Table 4.3: Mass in mg measured for one large grain of salt.

Test	Mass (mg)
1	0.5169
2	0.5184
3	0.5137
4	0.5057
5	0.4949
6	0.5280
7	0.5179
8	0.5196
9	0.5048
10	0.5069
11	0.4900
12	0.4966
13	0.4959
14	0.5098
15	0.5126
Average	0.5088
St dev.	0.0109

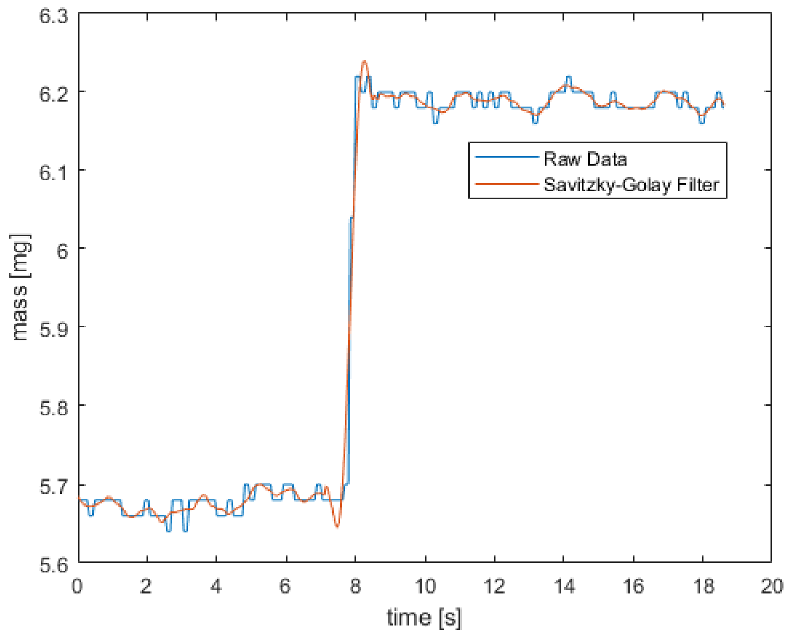

Figure 4.5: Wipotec response to one large salt grain dropped on the weigh cell.

Table 4.4: Mass in mg measured for one small grain of salt.

Test	**Mass (mg)**
1	0.0941
2	0.1156
3	0.1044
4	0.0984
5	0.1073
6	0.1050
7	0.0905
8	0.0928
9	0.0936
10	0.0941
11	0.1054
12	0.1053
13	0.0906
14	0.0892
15	0.0970
Average	0.0989
St dev.	0.0078

As seen in Figure 4.6, a noticeable jump is present again, indicating a force as low as 0.97 μN can be identified and accurately measured with a standard deviation of 0.08 μN. The grain was weighed on the Mettler digital balance three times and each measurement reading was 0.0001 g, or 0.1 mg, which is the resolution of the digital balance. This value matches the mass read out from the Wipotec of approximately 0.1 mg, within the resolution of the precision balance.

4.3 Effects of Minimum Thrust Level Experiment on μSTAMPS Design and Testing

The empirical results of the preceding Section demonstrated that thrust levels as low as 1 μN can be accurately detected and measured using the direct-measurement approach with a weigh cell. Low-mass nanosatellites such as 1U CubeSats may not need high thrust levels to reach certain mission requirements. For example, if a nanosatellite at lower altitudes in LEO does not require collision avoidance, such as in a swarm where an individual satellite's performance is not as important as the overall constellation, deorbit capabilities may be the most important use-case of a μSTAMPS thruster. The smaller mass and lower altitude may require only a small level of thrust to deorbit within the five-year requirement. With a smaller thrust requirement, the entire μSTAMPS assembly can be scaled down to fit this need, resulting in lower mass and power requirements associated with the propulsion system, and ultimately, result in a lower launch cost. The thrust levels for a scaled-down version of the μSTAMPS can be measured, ensuring adequate thrust for mission success.

The thrust produced from each capillary is estimated to be between 1 and 10 nN. With the minimum measurable thrust in mind, this estimate can be used to select the number of capillaries in the extraction grid to achieve a desired thrust level that is also measurable. The current μSTAMPS design includes 1,231 capillaries in the emitter chip.

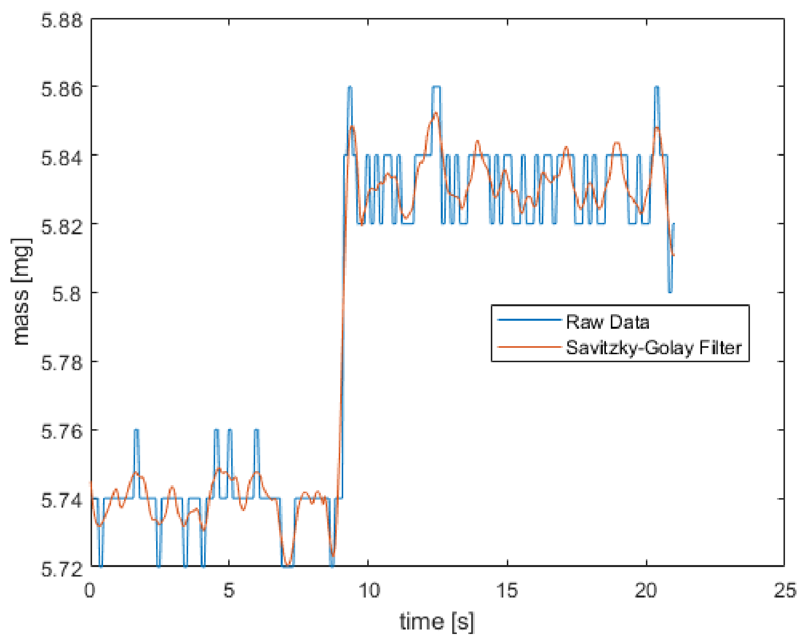

Figure 4.6: Wipotec response to one small salt grain dropped on the weigh cell.

With the current estimate, the μSTAMPS only needs between 100 and 1,000 capillaries to produce measurable thrust, so even at the lowest estimation, the thrust is measurable. Additionally, once a prototype is implemented with a certain number of capillaries, the measured thrust will allow for a more precise estimate for the thrust produced by each capillary to further improve accuracy for future scaling of the thruster.

Chapter 5

Conclusions and Future Work

5.1 Conclusions

As nanosatellite technology continues to grow and more nanosatellites are launched, the need for propulsion onboard increases exponentially. The FCC ruling requiring a deorbit within five years of mission end is an important driving factor when considering the necessity of propulsion for small satellites. The desire for collision avoidance and station keeping is also increasing this need. Furthermore, as nanosatellite technology continues to advance, deep-space missions become more feasible. These new opportunities necessitate the need for simplistic thrust measurement systems for the electrospray thrusters commonly used for such missions. With scalable thrusters, such as the μSTAMPS, testing will need to be frequent to deliver the promised thrust. A direct-measurement approach that bypasses complicated apparatus and calibration processes while remaining repeatable and accurate is necessary.

The direct-measurement approach imagined to meet this lofty goal involves the use of a microbalance capable of measuring the small forces exerted by ejected ions from an electrospray propulsion device. The Wipotec weigh cell is the selected balance for this set-up and the focus of this work. A series of baseline experiments were successfully conducted to ensure the weigh cell operated as intended. The test masses were measured accurately, and the settling time was verified in the work, along with an experiment evaluating the possible effect of an applied current, which mimics the situation of ionic capture during electrospray thruster operation.

The end goal of this Thesis was to determine a minimum level of thrust measurable from this approach. This was accomplished by dropping small grains of common table salt in decreasing numbers of grains to determine if and when the weigh cell was unable to resolve the force. The weigh cell was able to identify and accurately measure the force from dropping a single grain of salt, corresponding to approximately 1 μN. With this figure, the range for the minimum number of capillaries necessary on the extraction grid of the μSTAMPS was able to be determined before prototyping begins, of between 100 and 1,000 capillaries. The thrust level produced from each capillary can also be accurately determined once the prototype is fully implemented.

5.2 Future Work

The goal of this work was to determine the minimum thrust level that is measurable with the direct thrust-detection method using a weigh cell. While the force was easily resolved at the 1 μN level, a true minimum thrust level was not determined. The stated resolution of the Wipotec weigh cell is 0.02 mg so the theoretical minimum measurable thrust level should be 0.2 μN. To determine if this level of resolution is possible, the test would need to be repeated using objects with an even smaller mass on the order of, and ideally less than, the weigh cell's resolution limit of 0.02 mg. The chosen material would need to be large enough or have some other capacity to handle individual particles and have either known mass per particle of precise volume and density data in order to calculate the mass, but be light enough to determine the minimum force resolvable by the Wipotec weigh cell.

Furthermore, the next step is actual thrust characterization of a functioning μSTAMPS thruster using the thrust stand described in Section 1.4. This will help determine the true thrust produced per capillary and determine the efficiency of the system. Additionally, scaled versions of the capillary array on the emitter chip and full thruster assembly can be tested for completeness. It should be noted again here that to achieve practical thrust levels, additional acceleration will need to be applied to the ionic matter emitter by the μSTAMPS thruster chip, but this stage of development and analysis is beyond the scope of this Thesis.

The μSTAMPS thruster will be tested in a vacuum chamber to best simulate the environment in low Earth orbit that it will likely be operating in. Additional work will be required to determine if the passive damping on the thrust stand will be enough to overcome the noisy environment associated with vacuum testing, resulting from the vacuum pumps. Understanding the effect of the environment will be paramount in determining if the calibration process has truly been simplified for lower thrust-level thrusters and to fully characterize the μSTAMPS thruster. If it is determined that the environmental noise is too great, the μSTAMPS can be placed in the chamber and first pulled down to the working vacuum level, then the turbopump turned off temporarily for short-term thrust testing. Additional tests will be necessary to determine if turning off the pump will affect the Wipotec readouts, and if so, by how much, since there may be ionic matter emitted into the vacuum chamber not captured by the Faraday cup.

Bibliography

[1] Technical documentation for weigh cell series fs, 2019. Accessed: (4-6-2024). 24

[2] Density of iodized salt,. *Aqua-Calc*, 2020. https://www.aqua-calc.com/page/density-table/substance/iodized-blank-salt-coma-and-blank-upc-column–blank-041498131562. 40

[3] Dart's small satellite companion takes flight ahead of impact. *Johns Hopkins Applied Physics Laboratory*, 2022. 1

[4] Nasa's small spacecraft technology state of the art report. *Space daily*, 2023. xi, 4

[5] *Mitigation of Orbital Debris in the New Space Age*, volume 89. Federal Information News Dispatch, LLC, Washington, 2024. 2

[6] Ansys maxwell. NA. https://www.ansys.com/products/electronics/ansys-maxwell. 13

[7] Justin Jones, Alexander Terekhov, Brian Canfield, Lino Costa, and Trevor Moeller. Demonstration of dual mode ionic liquid propulsion. 2020. Final report to Streamline Automation, LLC for the NASA Phase 1 STTR award. 2, 21, 23

[8] Eric E. D'Ambro. Design of a thrust stand using impingement force on a weigh cell from an electric micro-propulsion thruster. 2023. Masters Project - University of Tennessee Space Institute. 16

[9] William Emrich. *Principles of nuclear rocket propulsion*. Amsterdam, 2016 - 2016. Elsevier ibsn: 0-12-804530-2. 19, 20, 21, 22, 23

[10] Michael Freemantle. An introduction to ionic liquids.(brief article). *CHOICE: Current Reviews for Academic Libraries*, 47(12):2356–, 2010. 5

[11] Manuel Gamero-Castaño. A torsional balance for the characterization of micronewton thrusters. *Review of scientific instruments*, 74(10):4509–4514, 2003. 13, 24

[12] Joshua H Howell. A numerical optimization study of a novel electrospray emitter design, 2022. Masters thesis - The University of Tennessee, Knoxville. xi, 4, 6

[13] Trevor Moeller, Lino Costa, Alexander Terekhov, Brian Canfield, Joshua Howell, Caitlin Bunce, Adam Huller, and Tyler Sundstrom. Concept design of µstamps thruster. *STTR Phase 1, SpaceWerx Topic n. AF-X21.S-CSO1 Proposal n. FX21S-TCSO1-0237*, 2022. xi, 5, 6, 7, 9

[14] Erik Kulu. World's largest database of nanosatellites, over 4000 nanosats and cubesats. *Nanosats Database*, 2024. 2

[15] James E Polk, Anthony Pancotti, Thomas Haag, Scott King, Mitchell Walker, Joseph Blakely, and John Ziemer. Recommended practice for thrust measurement in electric propulsion testing. *Journal of propulsion and power*, 33(3):539–555, 2017. 10, 11

[16] Kurt A. Polzin, Thomas E. Markusic, Boris J. Stanojev, Amado DeHoyos, and Benjamin Spaun. Thrust stand for electric propulsion performance evaluation. *Review of scientific instruments*, 77(10):105108–105108–9, 2006. 10

[17] Benjamin D. Prince, Bruce A. Fritz, and Yu-Hui Chiu. Ionic liquids in electrospray propulsion systems. In *Ionic liquids : science and applications*, Washington, DC, 2012. American Chemical Society. 5

[18] J. Soni and S. Roy. Design and characterization of a nano-newton resolution thrust stand. *Review of scientific instruments*, 84(9):095103–095103, 2013. xi, 13, 15, 24

[19] Marco Bisi, Paolo Cordiale, Enrico Canuto Stefano Cesare, Fabio Musso, Filippo D'Angelo, Giuseppe Castorina. Nanobalance: the european balance for micro-propulsion. *Electric Rocket Propulsion Society*, 2009. 10, 11

[20] George P. (George Paul) Sutton and Oscar. Biblarz. Rocket propulsion elements, 2010. Wiley ibsn: 9780470080245. 21, 22, 23

[21] Peter L. Wright, Henry Huh, Nolan M. Uchizono, Anirudh Thuppul, and Richard E. Wirz. A novel variable mode emitter for electrospray thrusters. *Electric Rocket Propulsion Society*, 2019. 5

[22] Kunning G Xu and Mitchell L. R Walker. High-power, null-type, inverted pendulum thrust stand. *Review of scientific instruments*, 80(5):055103–055103–6, 2009. xi, 10, 11, 12

[23] John K. Ziemer. Performance of electrospray thrusters. *Electric Rocket Propulsion Society*, 2009. 3

Vita

Caitlin Bunce was born and raised in North Carolina. She completed her bachelor's degree at UNC Charlotte in 2022, where she fell in love with space and rocketry after competing in, and winning, NASA's University Student Launch Initiative competition for the 2021-2022 season. Following the completion of her bachelor's degree, she continued on to pursue further education at the University of Tennessee Space Institute to earn a master's degree in aerospace engineering. She has worked as a graduate research assistant in the CEAR group for Dr. Trevor Moeller, Dr. Brian Canfield, and Dr. Lino Costa since September 2022 on a testing method for the μSTAMPS thruster for nanosatellites.